

Experimental and Theoretical Studies of the Charge Density Distribution in *E*-Tetraethyl-1,4-diammoniumbut-2-ene.2PF₆

KIRSTY L. MCCORMACK, PAUL R. MALLINSON,* BRIAN C. WEBSTER, DMITRII S. YUFIT, LINDSAY A. SLATER AND DAVID J. ROBINS

Chemistry Department, University of Glasgow, Glasgow G12 8QQ, Scotland. E-mail: paul@chem.gla.ac.uk

(Received 31 May 1996; accepted 10 September 1996)

Abstract

The [PF₆][−] salt of *E*-tetraethyl-1,4-diaminobut-2-ene has been synthesized and the crystal structure determined. The experimental electronic charge distribution has been obtained by fitting a multipole model to low-temperature, high-resolution, single-crystal X-ray diffraction data. A high-level *ab initio* molecular orbital calculation has also been performed for the cation, which is used as an antifungal agent. Both experimental and theoretical Laplacian distributions display maxima only at the bond critical points. This correlates with a calculated electrostatic potential which is positive at all points.

1. Introduction

Naturally occurring polyamines such as putrescine and spermidine are found in fungi and are essential for normal cell growth (Tabor, 1981). The cations of several putrescine derivatives have been synthesized (Havis, Walters, Martin, Cook & Robins, 1994) and found to exhibit considerable fungicidal activity against a range of plant pathogens. The exact reason for the activity of these putrescine analogues is unclear, although it has been suggested that it could be due to either the inhibition of polyamine biosynthesis or competitive binding to polyamine sites with the resultant disruption of structure (Porter & Suffrin, 1986).

Under physiological conditions the polyamines are largely protonated (Ganem, 1982) and the resulting cations carry a distributed positive charge which allows them to interact with anionic species. The polyamine cations interact with the negatively charged phosphate groups of DNA and it is thought that this interaction is the source of their antifungal activity (Walters, 1995). The nature of the polyamine/anion interaction is dependent upon the electrostatic potential surface of each ion. The characteristics of the potential surface of the polyamine cation, which in turn depend upon the distribution of the 2+ charge within the cation, are therefore of interest. A series of charge density studies of related polyamines of varying antifungal activity would therefore provide information from which structure/property relationships may be drawn. This study

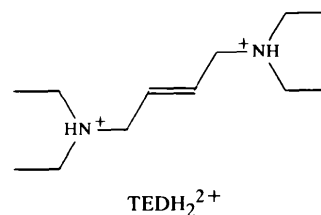
represents one of the first of such a series and its purpose is to investigate the electronic charge distribution of a polyamine cation with known fungicidal properties, [*E*-tetraethyl-1,4-diammoniumbut-2-ene]²⁺, TEDH₂²⁺. Very recently Cohen, Ruble & Craven (1996) reported a similar study of spermine phosphate hexahydrate.

It is also necessary to determine the electrostatic potential surface of the anion in order to confirm that an interaction with the anion is feasible. *Ab initio* molecular orbital calculations were therefore performed on the simplest model group which would approximate to the phosphate groups of the DNA helix, namely [PO₂(OCH₃)₂][−].

2. Experimental

2.1. Synthesis of *E*-tetraethyl-1,4-diammoniumbut-2-ene bis(hexafluorophosphate)

The synthesis of the free base was carried out by the general procedure of Biel & DiPierro (1958). *E*-Tetraethyl-1,4-diaminobut-2-ene, TED,



was dissolved in dry ether and a solution of HCl in ether was added. The resulting precipitate was filtered and washed with ether to give TEDH₂²⁺ dichloride as a white solid. Samples of the bis(hexafluorophosphate) were made by ligand exchange. TEDH₂²⁺ dichloride was dissolved in water and 1.2 equiv. of ammonium hexafluorophosphate in water was added. The resulting cream solid was filtered off and washed with water to give TEDH₂²⁺ bis(hexafluorophosphate); ν_{\max} (KBr disc), cm^{−1}: 3425.9 (N—H), 972.2 [(*E*) HC=CH], 838.0 (P—F); ¹³C NMR (CD₃OD): 8.6 (CH₃), 47.9 (CH₂—CH₃), 52.8 (CH₂—CH), 129.4 (CH); *m/z* 200

($M^+ - 2PF_6$, 2.3%), 126 (76.0%), 110 (13.2%), 86 (100%), 72 (74.8%), 56 (62.3%), 42 (47.7%). Crystals suitable for this study were grown from a solution of methanol/ether and obtained as colourless plates (m.p. 462–462.5 K).

2.2. X-ray data collection

Single-crystal, high-resolution, low-temperature data were collected using the same equipment as described in an earlier paper (Howard, Hursthouse, Lehmann, Mallinson & Frampton, 1992). Data reduction was performed with the *DREADD* program package (Blessing, 1989). The intensities of standard reflections were fitted to cubic polynomials, which were used for scaling the data. The crystal faces were indexed, the two largest faces having indices of 100 and $\bar{1}00$; the sides were bounded by the 011, $0\bar{1}\bar{1}$, $01\bar{1}$ and $0\bar{1}1$ faces. This information was used to perform a Gaussian analytical correction for absorption by the crystal using *ABSORB* (DeTitta, 1984). Thermal diffuse scattering was not corrected for.

2.3. Molecular orbital calculations

Ab initio molecular orbital calculations were performed for the cation at the crystalline geometry, and also for the model phosphate group, in order to gain

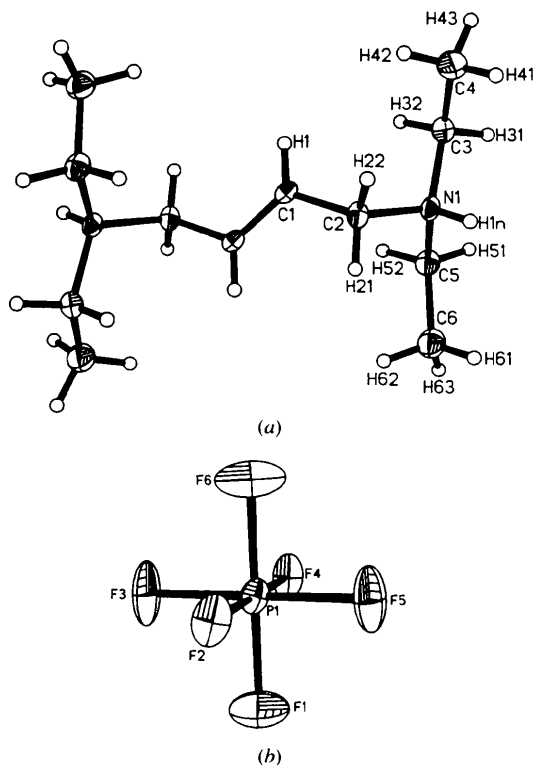


Fig. 1. (a) The crystallographically centrosymmetric structure of $TEDH_2^+$. (b) The PF_6^- anion. Thermal ellipsoids are drawn at 50% probability.

information about the electronic charge distribution of these species. The geometry of the model system, $[PO_2(OCH_3)_2]^-$, was optimized. All *ab initio* calculations were performed using the *GAMESS* program (Schmidt *et al.*, 1993) at the HF-SCF 6-311G** level. The critical point information and Laplacian map of the polyamine cation were obtained from the HF-SCF wavefunction using the *AIMPAC* suite of programs (Biegler-König, Bader & Tang, 1982). The electrostatic potential maps were plotted with the *MEPMAP* program of the graphics package of *GAMESS* (Schmidt *et al.*, 1993).

2.4. Multipole refinement

The crystal structure was solved using *SHELXS86* (Sheldrick, 1985) and refined with *SHELXL93* (Sheldrick, 1993). At room temperature the $[PF_6]^-$ group is disordered, four of the F atoms appearing as a 'spinning wheel' around the F2—P—F4 axis. This is dynamic disorder as no significant disorder is observed at low temperature. The space group requires the cation in the crystal to have point symmetry C_i , the centre of inversion being located at the midpoint of the C—C double bond, Fig. 1. The computational details of the multipole refinement are as reported in an earlier paper by McCormack, Mallinson, Webster & Yufit (1996). The refinement was performed using the program *XDLSM* of *XD* (Koritsansky *et al.*, 1995).

An overall electroneutrality constraint was applied to the monopole charges. In addition, the anions and cation were constrained to have net charges of -1 and $+2$, respectively.

In this refinement the expansion was truncated at the hexadecapole level ($l_{max} = 4$) for all non-H atoms. This level of expansion was considered to be reasonable as there was significant occupation of the hexadecapoles on all non-H atoms. For H atoms the expansion was truncated at the $l_{max} = 1$ level, using one bond-directed dipole per H atom. Significant occupation of the other two dipoles was not observed and so they were removed from the expansion in order to improve the observations-to-variables ratio.

Separate κ' and κ'' were employed for each non-H atom type. It was thought initially that partitioning the C atoms into chemically equivalent sets, which would each have separate κ' and κ'' parameters, might improve the description of the ethyl groups. It was found, however, that the carbon κ sets refined to values which were not significantly different from each other. The C atoms were therefore assigned to the same κ set in order to improve the observations-to-variables ratio. For H atoms κ' and κ'' were fixed at 1.2, an average value obtained from theoretical models (Howard, 1992). Values of κ'' were initially fixed at 1.0 for non-H atoms, but were allowed to vary after all other parameters had been refined. The κ'' values for the four sets of multipoles ($1 \leq l \leq 4$) in

Table 1. *Experimental details*

Crystal data	
Chemical formula	C ₁₂ H ₂₈ F ₁₂ N ₂ P ₂
Chemical formula weight	490.3
Cell setting	Monoclinic
Space group	P2 ₁ /c
<i>a</i> (Å)	6.282 (1)
<i>b</i> (Å)	13.252 (1)
<i>c</i> (Å)	13.112 (1)
β (°)	98.08 (9)
<i>V</i> (Å ³)	1079.5 (2)
<i>Z</i>	2
<i>D_c</i> (Mg m ⁻³)	1.51
Radiation type	Mo Kα
Wavelength (Å)	0.71069
No. of reflections for cell parameters	25
θ range (°)	13–15
μ (mm ⁻¹)	0.300
Temperature (K)	100
Crystal form	Plate
Crystal size (mm)	0.3 × 0.3 × 0.1
Crystal colour	Colourless
Data collection	
Diffractometer	Enraf–Nonius CAD-4
Data collection method	ω–2θ scans
Absorption correction	Gaussian quadrature (DeTitta, 1984)
<i>T_{min}</i>	0.931
<i>T_{max}</i>	0.979
No. of measured reflections	19 338
No. of independent reflections	6884
No. of observed reflections	3611
Criterion for observed reflections	<i>I</i> > 2σ(<i>I</i>)
<i>R_{int}</i>	0.034
θ _{max} (°)	55
Range of <i>h</i> , <i>k</i> , <i>l</i>	–15 → <i>h</i> → 15 –24 → <i>k</i> → 24 –12 → <i>l</i> → 23
No. of standard reflections	6
Frequency of standard reflections (min)	120
Intensity decay (%)	None
Refinement	
Refinement on	<i>F</i>
<i>R</i>	0.021
<i>wR</i>	0.022
<i>S</i>	1.003
No. of reflections used in refinement	3611
No. of parameters used	513
H-atom treatment	See text
Weighting scheme	$w = 4F^2/[\sigma^2(F^2) + 0.0006F^4]$
(Δ/σ) _{max}	0.1
Δρ _{max} (e Å ⁻³)	0.3
Δρ _{min} (e Å ⁻³)	–0.2
Source of atomic scattering factors	<i>International Tables for X-ray Crystallography</i> (1974, Vol. IV, Tables 2.2B and 2.3.1)
Computer programs	
Data collection	CAD-4 Express (Enraf–Nonius, 1992)
Cell refinement	CAD-4 Express (Enraf–Nonius, 1992)
Data reduction	DREADD (Blessing, 1989)
Structure solution	SHELXS86 (Sheldrick, 1985)
Structure refinement	SHELXL93 (Sheldrick, 1993) and XD (Koritsanzky <i>et al.</i> , 1995)
Preparation of material for publication	XD (Koritsanzky <i>et al.</i> , 1995)

each κ set were constrained to have the same value. The final κ values are: $\kappa'_C, \kappa''_C = 0.963$ (4), 0.835 (6); $\kappa'_N, \kappa''_N = 0.99$ (1), 0.84 (3); $\kappa'_P, \kappa''_P = 1.03$ (1), 0.71 (1); $\kappa'_F, \kappa''_F = 0.979$ (2), 1.03 (1).

Table 2. *Fractional atomic coordinates and equivalent isotropic displacement parameters (Å²)*

$$U_{eq} = (1/3)\sum_i\sum_j U^{ij} a_i^* a_j^* \mathbf{a}_i \cdot \mathbf{a}_j.$$

	<i>x</i>	<i>y</i>	<i>z</i>	<i>U_{eq}</i>
P1	–0.54040 (2)	0.32589 (1)	0.81703 (1)	0.015
F1	–0.5598 (4)	0.4123 (3)	0.7306 (2)	0.037
F2	–0.28358 (19)	0.32999 (14)	0.82658 (14)	0.024
F3	–0.5454 (3)	0.2391 (2)	0.7293 (2)	0.034
F4	–0.80117 (19)	0.31994 (14)	0.80455 (13)	0.024
F5	–0.5399 (3)	0.4124 (2)	0.9030 (2)	0.035
F6	–0.5249 (4)	0.2415 (2)	0.9055 (3)	0.042
N1	0.03394 (14)	0.15113 (7)	0.66671 (7)	0.013
C1	0.02006 (13)	0.00150 (7)	0.55129 (6)	0.014
C2	0.16022 (12)	0.08027 (6)	0.60768 (7)	0.014
C3	–0.07967 (15)	0.09909 (7)	0.74585 (8)	0.018
C4	0.0703 (2)	0.0368 (1)	0.8213 (1)	0.026
C5	–0.12225 (14)	0.21602 (7)	0.59781 (7)	0.017
C6	–0.01186 (18)	0.28627 (8)	0.53094 (8)	0.023

Bond lengths to hydrogen were fixed at the average values obtained from neutron diffraction by Allen *et al.* (1987), 1.06 Å for the C–H bond and 1.033 Å for the N–H bond. The bond directions and H-atom isotropic temperature factors were fixed at values obtained from an independent atom model refinement, in which all atoms were treated as spherical.

The Laplacian map and the critical point information were obtained using the program *XDPROP* in the *XD* package.

3. Results

Details of the final *R* factors and goodness-of-fit for the 3611 reflections used in the multipole refinement are given in Table 1. The observations-to-variables ratio is 7. Atomic coordinates are given in Table 2 and anisotropic displacement parameters are shown in Table 3.*

Figs. 2(a) and (b) show the residual density maps for the cation and anion, respectively. Fig. 3 shows a theoretical electrostatic potential map of TEDH₂²⁺ in the plane defined by the two N atoms and the midpoint of the C–C double bond. The map for the model phosphate group is shown in Fig. 4; the plane is that defined by the PO₂ fragment.

Table 4 shows the chemical shifts for the ¹H NMR spectra of the free base, TED, and for TEDH₂²⁺. Valence monopole and Mulliken charges from the experimental and theoretical charge density studies, respectively, are shown in Table 5. The results of the critical point analyses are listed in Table 6. The experimental and theoretical Laplacian maps for the carbon–carbon double bond are shown in Figs. 5(a) and (b), respectively.

* Lists of structure factors, complete geometry, multipole population coefficients and local coordinate systems have been deposited with the IUCr (Reference: CF0001). Copies may be obtained through The Managing Editor, International Union of Crystallography, 5 Abbey Square, Chester CH1 2HU, England.

Table 3. Mean-square atomic displacements (\AA^2)The form of the anisotropic displacement factor is: $\exp[-2\pi^2 \sum_i \Sigma_j U^{ij} h_i h_j a_i^* a_j^*]$

	U^{11}	U^{22}	U^{33}	U^{12}	U^{13}	U^{23}
P1	0.0106 (1)	0.0150 (1)	0.0185 (1)	-0.0016 (1)	0.0024 (1)	-0.0044 (1)
F1	0.0299 (8)	0.0390 (10)	0.0404 (10)	0.0002 (8)	0.0048 (8)	0.0155 (9)
F2	0.0104 (4)	0.0268 (6)	0.0341 (7)	-0.0034 (4)	0.0025 (4)	-0.0107 (6)
F3	0.0141 (5)	0.0388 (8)	0.0490 (9)	-0.0043 (6)	0.0075 (6)	-0.0308 (8)
F4	0.0107 (4)	0.0294 (6)	0.0311 (6)	-0.0021 (4)	0.0051 (4)	-0.0134 (6)
F5	0.0236 (7)	0.0420 (9)	0.0405 (9)	-0.0098 (7)	0.0125 (7)	-0.0260 (9)
F6	0.032 (1)	0.048 (1)	0.043 (1)	-0.012 (1)	-0.004 (1)	0.021 (1)
N1	0.0137 (3)	0.0120 (3)	0.0143 (4)	-0.0006 (2)	0.0022 (3)	-0.0030 (2)
C1	0.0152 (3)	0.0119 (3)	0.0138 (3)	-0.0015 (2)	0.0028 (3)	-0.0017 (3)
C2	0.0119 (3)	0.0145 (3)	0.0169 (3)	-0.0006 (2)	0.0027 (2)	-0.0038 (3)
C3	0.0207 (3)	0.0165 (3)	0.0180 (4)	-0.0007 (3)	0.0071 (3)	-0.0011 (3)
C4	0.0371 (5)	0.0198 (4)	0.0208 (4)	0.0040 (4)	0.0057 (4)	0.0032 (4)
C5	0.0167 (3)	0.0165 (3)	0.0184 (4)	0.0024 (3)	0.0031 (3)	-0.0008 (3)
C6	0.0287 (4)	0.0195 (4)	0.0195 (4)	-0.0006 (4)	0.0038 (3)	0.0024 (3)
H1N	0.022					
H1	0.030					
H21	0.034					
H22	0.021					
H31	0.025					
H32	0.015					
H41	0.031					
H42	0.039					
H43	0.042					
H51	0.021					
H52	0.025					
H61	0.053					
H62	0.034					
H63	0.051					

4. Discussion

The residual density maps, Figs. 2(a) and (b), show randomly distributed regions of low residual density, indicating that the electron distribution is satisfactorily described by the multipole model. Application of the rigid-bond test (Hirshfeld, 1976) shows that three of the bonds in the anion, P1—F1, P1—F5 and P1—F6, have differences in mean-square displacement amplitudes in the bond directions slightly greater than 0.001\AA^2 , which may be related to larger than normal displacement amplitudes for these F atoms (Table 3), perhaps due to a small degree of residual disorder of the $[\text{PF}_6]^-$ group. All bonds in the cation satisfy the test criterion.

The shortest interionic distances correspond to hydrogen-bond interactions between H1N of the cation and F3 and F4 of an anion related by the symmetry operation $x - 1, y, z$. These distances are $1.993(1)$ and $2.050(1) \text{\AA}$, respectively, and the N1—H1N—F3/F4 angles are $144.7(1)$ and $146.9(1)^\circ$. The bond critical point of such an interaction is typically characterized by a low value of the total density and a positive Laplacian, which is found to be the case here. The critical point information for these bonds is shown in Table 6.

The atomic charges within the cation (Table 5), relevant to the polyamine-phosphate interaction, show differences in magnitudes between the experimental valence monopole and theoretical Mulliken values. This is due to the different partitioning of the molecular charge in the two cases (Mulliken, 1955; Stewart, 1976).

Table 4. ^1H NMR data for TED and TEDH_2^{2+} , δ values in ppm

All spectra were carried out in CD_3OD with TMS as an internal standard.

Proton environment	TED	TEDH_2^{2+}	Δ (ppm)
CH_2-CH_2	1.04	1.32	+0.28
$\text{CH}_3-\text{CH}_2-\text{N}$	1.54	3.22	+0.68
$\text{N}-\text{CH}_2-\text{CH}$	3.12	3.88	+0.76
CH	5.70	6.15	+0.45

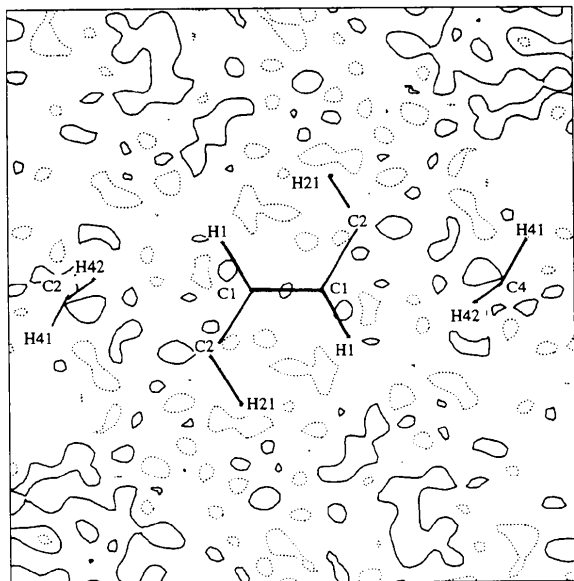
However, a qualitative comparison can be made and would be expected to show the same general trends in both sets of results. The experimental and theoretical charges both show the C and N atoms to carry partial negative charges, whilst all the H atoms are positively charged. This is confirmed by the ^1H NMR spectra of the non-protonated form of the molecule, TED, and of TEDH_2^{2+} , see Table 4. In TEDH_2^{2+} each of the N atoms carries a formal positive charge and so they act as powerful electron-withdrawing groups. As a result the +2 charge is not located on the nitrogens, but is distributed over the H atoms and the proton environments in the cation are thus deshielded, leading to downfield shifts in δ , *i.e.* higher values of δ .

The shift is largest for those protons bonded to C atoms which are α to nitrogen as here the effect will be greatest; as expected, the shift of the methylene protons next to a nitrogen is of the order $+0.7$ p.p.m. The effect is still appreciable for protons on carbons β to the N

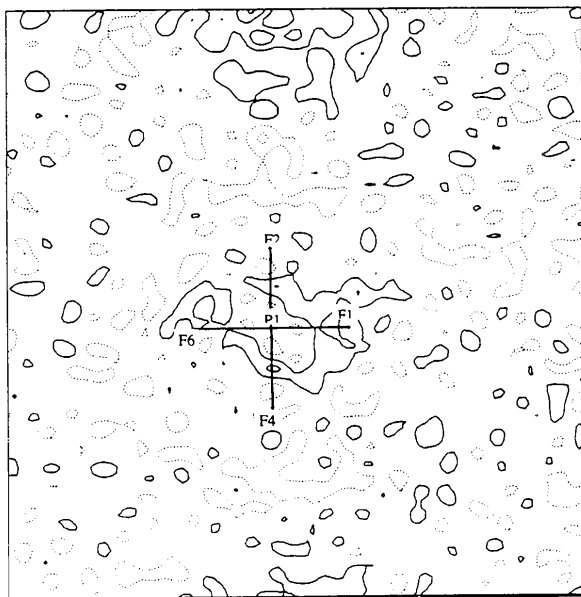
atom. The relative magnitudes of the charge depletion can be compared with those obtained from the valence monopole charges. The proton NMR shows the largest electron depletion to be on the H atoms bonded to C2, followed by those bonded to C3/C5, C1 and C4/C6 in order of decreasing electron depletion of the proton. The ^1H NMR averages the environments of the chemically

Table 5. Atomic charges for the atoms in TEDH_2^{3+}

	Atomic charge (electrons)	
	Valence monopole	Mulliken
C1	-0.245	-0.067
C2	-0.344	-0.009
N1	-0.040	-0.394
C3	-0.329	-0.068
C4	-0.585	-0.146
C5	-0.439	-0.053
C6	-0.588	-0.145
H1	0.240	0.078
H1N	0.332	0.277
H21	0.219	0.146
H22	0.278	0.174
H31	0.241	0.151
H32	0.287	0.132
H41	0.332	0.110
H42	0.198	0.079
H43	0.237	0.140
H51	0.364	0.144
H52	0.255	0.135
H61	0.185	0.110
H62	0.258	0.076
H63	0.106	0.129



(a)



(b)

Fig. 2. Residual density for: (a) the cation in the plane $\text{C2}-\text{C1}-\text{C1}'-\text{C2}'$; (b) the anion in the plane $\text{F1}-\text{P1}-\text{F2}$. Contour interval $0.1 \text{ e } \text{\AA}^{-3}$, solid lines are positive contours, dotted lines are negative. Here and elsewhere the prime denotes an atom related by crystallographic inversion (symmetry operator $-x, -y, 1 - z$).

equivalent protons. Averaging the chemically equivalent monopole charges gives the sequence: H atoms bonded to C3/C5 followed by C2, C1 and C4/C6. The H atoms on carbons α to nitrogen are thus reordered.

Both experiment and theory show the proton with the largest positive charge to be that bonded to N1. That

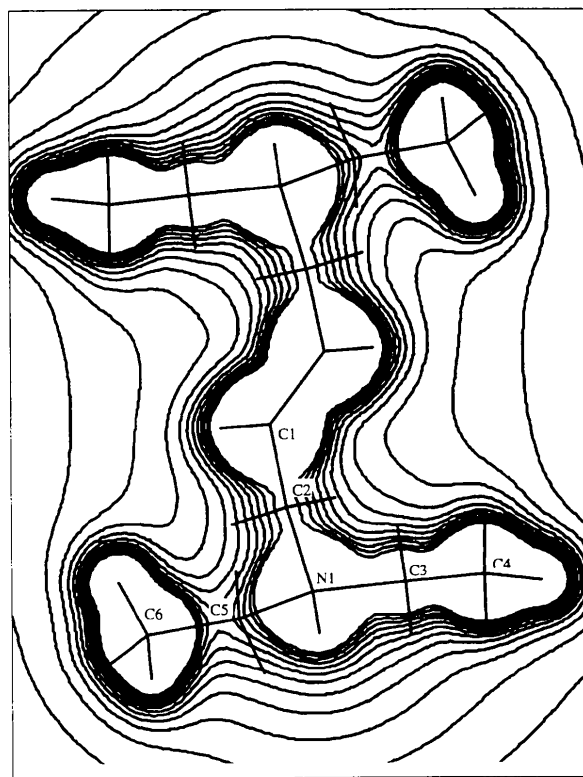


Fig. 3. Map of the theoretical electrostatic potential of the TEDH_2^{3+} ion, in the plane of N1 , C1 and $\text{C1}'$. Contour interval 100 kJ mol^{-1} .

Table 6. Critical point data for selected bonds

Atoms	Bond length (Å)	ρ ($e \text{ \AA}^{-3}$)	Experimental Laplacian ($e \text{ \AA}^{-5}$)	Ellipticity	ρ ($e \text{ \AA}^{-3}$)	Theoretical Laplacian ($e \text{ \AA}^{-5}$)	Ellipticity
C1—C1'	1.334 (2)	3.01 (9)	-44.3 (3)	0.47	2.41	-27.9	0.43
C1—C2	1.493 (2)	2.13 (6)	-26.9 (2)	0.14	1.86	-19.4	0.02
C2—N1	1.511 (2)	1.84 (7)	-22.3 (3)	0.11	1.56	-10.8	0.11
N1—C3	1.507 (2)	1.83 (9)	-22.6 (5)	0.42	1.52	-5.3	0.12
C3—C4	1.512 (2)	2.00 (6)	-26.4 (2)	0.40	1.76	-17.4	0.01
N1—C5	1.506 (2)	1.76 (9)	-25.4 (5)	0.15	1.52	-5.8	0.14
C5—C6	1.512 (2)	2.11 (6)	-25.0 (2)	0.07	1.76	-17.5	0.01
H1N—F3	1.994 (2)	0.09 (2)	2.1 (1)	0.38			
H1N—F4	2.050 (2)	0.08 (1)	1.7 (1)	0.58			

is with the exception of H51 in the experiment, which has a valence monopole charge not significantly different from that of H1N.

The N atoms should carry a greater negative charge than the C atoms, considering that a formally positive N atom is extremely electronegative. This is found to be the case in theory, but not from experiment.

It is difficult to predict the nature of intermolecular interactions from atomic charges alone, particularly in this case where the experimental and theoretical values disagree in the respect mentioned above. Theoretical electrostatic potential maps were therefore plotted for $TEDH_2^{2+}$ and for the model phosphate group. The negative charges on the C and N atoms might disfavour an interaction with the negatively charged phosphate. It appears that these charges are small and diffuse enough not to feature as regions of negative potential. In fact, the whole of the potential surface of $TEDH_2^{2+}$ is shown to be positive, Fig. 3.

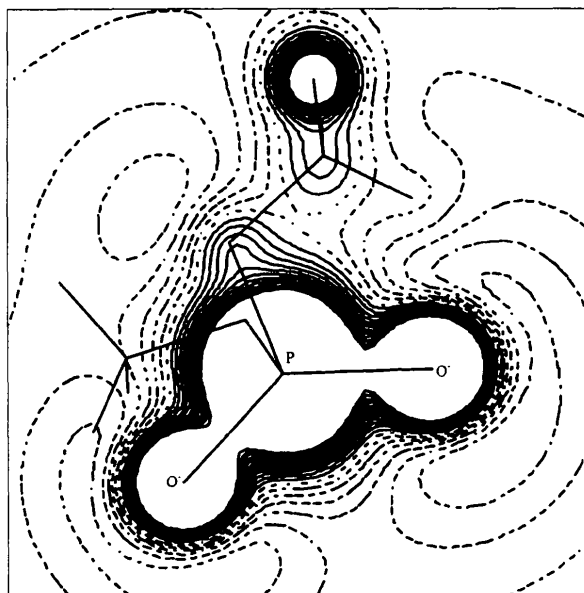
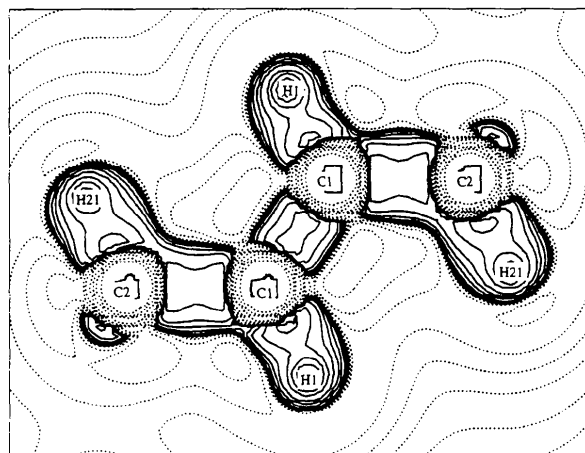
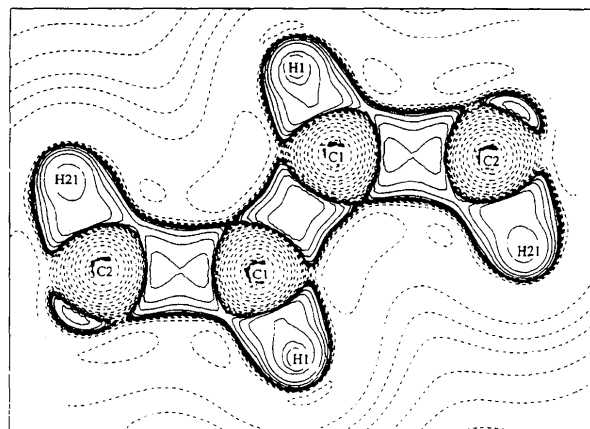


Fig. 4. Map of the electrostatic potential of the model phosphate group $[PO_2(OCH_3)_2]^-$, in the plane O—P—O. Contours are plotted at intervals of 100, from -700 to 1200 kJ mol^{-1} . Solid lines are positive contours, dashed lines are negative.

The electrostatic potential map of the model phosphate group (Fig. 4) shows large regions of negative potential, -700 kJ mol^{-1} , associated with the lone-pair electrons of the O atoms. We predict a strong intermolecular interaction between the polyamine cation and the DNA phosphate group, simply because of the opposite charges. Possibly this interaction is not site-specific with



(a)



(b)

Fig. 5. Laplacian distribution of $TEDH_2^{2+}$ in the plane defined by the central C atoms: (a) experimental; (b) theoretical. Contours at logarithmic intervals in $-\nabla^2 \rho^2 e \text{ \AA}^{-5}$.

respect to TEDH_2^+ as all points on the surface have large positive potentials. It is interesting to note that a similar conclusion was reached by Cohen, Ruble & Craven (1996) concerning the interaction of spermine with the phosphate groups of DNA.

We now come to the key point of this discussion. The charge density distributions resulting from both the multipole model and the *ab initio* calculation were analysed using Bader's treatment of the topology of the charge density (Bader, 1990; Table 6). Maps of the negative Laplacian in the C1—C1' region (across the inversion centre) for both the experimental and theoretical charge distributions are shown in Figs. 5(a) and (b). There is very good agreement between the two. The Laplacian value at the C—C double-bond critical point is more negative than in the C—C and C—N single bonds. The topology of the three-dimensional Laplacian distribution, as distinct from that of the charge density itself, exhibits no maxima, *i.e.* (3,−3) critical points, such as are normally associated with atomic lone pairs. The absence of charge concentrations, other than those associated with bonds, is as expected from the theoretical electrostatic potential map which shows the cation to have a continuous positive potential surface.

ρ_b for the C=C double bond has a high value, as is expected for a multiple bond. The ellipticity of this bond is close to 0.5, the value predicted for a pure carbon-carbon double bond. The experimental values for the ellipticities of the N1—C3 and C3—C4 bonds, around 0.4, are anomalous, while the theoretical values are in accord with expectation for single bonds. In the second ethyl group, the N1—C5 and C5—C6 bonds have experimental and theoretical ellipticity values close to zero, so that in the theoretical results the two ethyl groups are equivalent with ellipticities for all of the bonds (N1—C3, C3—C4, N1—C5, C5—C6) close to zero. Whilst the experimental results show a marked difference in the ellipticities of the two ethyl groups, there is no significant difference between either the values of the total density or the Laplacian at the bond critical points in the two ethyl groups. This, together with the generally good agreement with theory, leads us to believe that the multipole model chosen gives a satisfactory description of the charge density distribution. We are not able to explain the anomalous ellipticities, but they are unlikely to be due to the effect of intermolecular interactions, as no substantial differences between contacts involving the two ethyl groups are apparent. Neither is the discrepancy between the two ethyl groups due to excessive motion of the N1—C3—C4 group, as the rigid-bond test is satisfied.

5. Conclusions

Multipole analysis of the charge density distribution of TEDH_2^+ supports the conclusion from the *ab*

initio molecular orbital calculation that the electrostatic potential is positive at all points on the surface of the cation. We hope that these investigations will prove fruitful in the modelling of interactions associated with the antifungal activity of the cation.

We thank the EPSRC for a research fellowship for DSY (GR/J 22702) and a postgraduate studentship for KLM (94310222) and we also thank The Wellcome Trust for a postgraduate studentship for LAS.

References

- Allen, F. H., Kennard, O., Watson, D. G., Brammer, L., Orpen, A. G. & Taylor, R. (1987). *J. Chem. Soc. Perkin Trans. 2*, pp. S1–S19.
- Bader, R. F. W. (1990). *Atoms in Molecules: A Quantum Theory*. Oxford University Press.
- Biegler-König, F. W., Bader, R. F. W. & Tang, T. (1982). *J. Comput. Chem.* **3**, 317–328.
- Biel, J. H. & DiPierro, F. (1958). *J. Am. Chem. Soc.* **80**, 4609–4614.
- Blessing, R. H. (1989). *J. Appl. Cryst.* **22**, 396–397.
- Cohen, A. E., Ruble, J. R. & Craven, B. M. (1996). *Acta Cryst.* **A52**, C-261.
- DeTitta, G. (1984). *ABSORB*. Medical Foundation of Buffalo, USA.
- Enraf-Nonius (1992). *CAD-4 Express*. Version 5.1. Enraf-Nonius, Delft, The Netherlands.
- Ganem, B. (1982). *Acc. Chem. Res.* **15**, 290–298.
- Havis, H. D., Walters, D. R., Martin, W. P., Cook, F. M. & Robins, D. J. (1994). *Pestic. Sci.* **41**, 71–76.
- Hirshfeld, F. L. (1976). *Acta Cryst.* **A32**, 239–244.
- Howard, S. T. (1992). Personal communication.
- Howard, S. T., Hursthouse, M. B., Lehmann, C. W., Mallinson, P. R. & Frampton, C. S. (1992). *J. Chem. Phys.* **97**, 5616–5630.
- Koritsansky, T., Howard, S. T., Richter, T., Mallinson, P. R., Su, Z. & Hansen, N. K. (1995). *XD. A Computer Program Package for Multipole Refinement and Analysis of Charge Densities from Diffraction Data*. Berlin, Cardiff, Glasgow, Buffalo, Nancy.
- McCormack, K. L., Mallinson, P. R., Webster, B. C. & Yufit, D. S. (1996). *Faraday Trans.* **92**, 1709–1716.
- Mulliken, R. S. (1955). *J. Chem. Phys.* **23**, 1833–1846.
- Porter, C. W. & Suffrin, J. R. (1986). *Anticancer Res.* **6**, 525–542.
- Schmidt, M. W., Baldrige, K. K., Boatz, J. A., Elbert, S. T., Gorgon, M. S., Jensen, J. J., Koseki, S., Matsunaga, N., Nyugen, K. A., Su, S., Windus, T. L., Dupuis, M. & Montgomery, J. A. (1993). *J. Comput. Chem.* **14**, 1347–1363.
- Sheldrick, G. M. (1985). *SHELXS86. Program for the Solution of Crystal Structures*. University of Göttingen, Germany.
- Sheldrick, G. M. (1993). *SHELXL93. Program for Crystal Structure Refinement*. University of Göttingen, Germany.
- Stewart, R. F. (1976). *Acta Cryst.* **A32**, 565–574.
- Tabor, C. W. (1981). *Med. Biol.* **59**, 272–278.
- Walters, D. R. (1995). *Mycol. Res.* **99**, 129–139.